Engineering Solid Mechanics 9 (2021) 377-390

Contents lists available at GrowingScience

Engineering Solid Mechanics

homepage: www.GrowingScience.com/esm

Development of a nomogram to predict the contact stress between an I-girder and a support roller

Thanin Chanmalai[a], Byungik Chang[b*], Kevin Misaro[a], Saron Hagos[a] and Thippesh Bethur Hanumanthareddy[a]

[a]*Research Assistant, Department of Civil and Environmental Engineering, University of New Haven, West Haven, Connecticut, 06516, United States*
[b]*Associate Professor of Civil Engineering, Department of Civil and Environmental Engineering, University of New Haven, West Haven, Connecticut, 06516, United States*

ARTICLEINFO

Article history:
Received 11 April 2021
Accepted 6 July 2021
Available online
6 July 2021

Keywords:
Incremental Launching Method
Contact Stress
Hertz Contact theory
Numerical Modeling
Nomogram

ABSTRACT

The incremental launching method (ILM) is an efficient method of bridge construction primarily suited for environmentally sensitive areas. However, during the bridge launching, there are significant contact stresses between the launching system and the steel bridge girders. These substantial contact stresses can cause damage both on, and just under, the girder surface. Although Hertz contact theory solutions may give an insight into the problem, the accuracy is uncertain due to the presence of complex geometries, loads, and material properties. The complicated structural systems need to rely on numerical modeling such as the finite element analysis which are not always available. The primary objective of this study is to estimate the relationship of the maximum contact stress between an I-girder and a roller using a nomogram. The nomogram is built based on a parametric study with various roller dimensions and loads by numerical modeling. The maximum contact stress from the nomogram can be a useful tool in designing a bridge girder on a support roller.

1. Introduction

A bridge superstructure installed using the incremental launching method (ILM) is constructed on one side/abutment to be crossed and then launched into its final state. The launching is typically delivered in a range of increments thereby allowing additional sections to be added to the rear of the superstructure unit before subsequent launches. A viable example is the Iowa River Bridge (IRB), on Highway 20 in north-central Iowa crossing an environmentally sensitive river belt, which was constructed by the ILM to minimize the environmental impacts (Wipf et al., 2004). During bridge launching, there are significant forces that can be generated between the launching system and the steel I-girder. When one or both of the surfaces in contact are coated, the effect of surface roughness on wear is even more complex. The topography of both surfaces in contact often has a crucial influence on both friction and wear in dry and lubricated tribological contacts (Laukkanen et al., 2017). As expected, high contact stresses would be created at the point of contact between the roller and the lower surface of I-girder. The described small contact area with the reactions on the roller can cause severe damage to the structure. Hertz contact theory is not applicable to the solutions of contact stress problems with closed-form solutions because of the complicated geometries, loadings, and material properties in this case (Hertz, 1896). The

* Corresponding author. Tel.: +1-203-343-3468
E-mail addresses: bchang@newhaven.edu (B. Chang)

doi: 10.5267/j.esm.2021.7.001

aforementioned theory is based on the assumption that the contacting surfaces between the two geometries are: frictionless; the stress and strain of homogeneous materials occur within the elastic limit; and the load is applied perpendicular to the surface (Norden, 1973).

The contact stress analysis in a complicated structural system needs to rely on numerical modeling. Much research has been performed using a numerical modeling approach to solve the contact problem. Zhao and Li (2014) applied numerical modeling to solve the frictional wheel-rail rolling contact. Many factors contribute to rolling contact failure, such as the contact forces, steady/non-steady effects, plasticity and residual stresses, the ratcheting behavior, and contact surface roughness (Olver, 2005 and Donzella & Petrogalli, 2010). Additionally, the load length as denoted in Hertz contact stress theory plays a critical role in determining the magnitude of the eventual contact stress (Rogač et al., 2020 & 2021). The aforementioned load length, coupled with the conceptualized dimensioning of the I-Girder, determines whether the contact stress may result in overall system failure (Gąska et al., 2017). Cyclic stress and plastic deformation are among the dominant influencing factors. When the contact force exceeds a certain limit, cyclic plastic deformation and residual stresses and strains develop. The cyclic deformation promotes microstructure changes and results in the failure of wheels and rail. Hence, accurate stress analysis is crucial to understand wheel–rail rolling contact failures. Wen et al. (2010) focused on the distribution of surface shear stress and micro-slip development in the contact patch to investigate the relationships between material properties, plastic deformation, frictional contact, wear, and crack initiation. Wriggers (1996) approached numerical modeling with friction when general constitutive equations are formulated in the contact interface. Applying a geometrical model and discretization for contact was validated for large deformations. A finite element modeling of a spur gear assembly was developed by Gupta et al. (2012) to compare the contact stress between two gears with the Hertz contact stress theory equation. Based on the result of the contact stress analysis, parametric models were created for the design of gear.

The maximum contact stress decreases by increasing the geometric size. Numerical modeling validated the simulation results, in terms of Hertz contact theory, with the theoretical data of the involute tooth of a spur gear and the research showed that the validation of the contact stress was accurate (Bekheet, 2017). The behavior of girder webs subjected to a local load with a concentrated load perpendicular to the flange on a plate girder occurs during the launching of the bridge. Projected failure behavior can be determined by the slenderness of the steel girder and the load condition. The investigated girder dimensions and the moment capacity of the flange do not influence the bearing capacity from the local load, however, the bending stiffness of the flange is used to determine the resistance (Granath, 1997). The distribution of support reactions against a steel girder on a launching shoe using laboratory experiments, finite element analysis, and mathematical calculation was estimated by Granath. These three features are involved with the reaction force when the steel girder is launched on a launching shoe with a slide bearing. The design calculations for the appropriate load are performed with equations valid for the case of a uniform distribution. The study showed that the support reaction has a non-uniform distribution of contact stress (Granath, 1998). Moreover, an experiment in a reducing scale test of I-shaped steel girder bridge was conducted by Chacon et al. and the results including strains, stresses, and displacements during launching were validated by the numerical modeling (Chacón, 2013). Chang studied the behavior of Iowa River Bridge and focused on the contact stress between the steel I-girder and a support roller during launching using numerical modeling. Chang (2004a) considered the member-end force-based approach, girder aspect ratio to minimize the modeling size, hexahedral mesh, material nonlinearity in his study. However, Chang made an initial bonded condition between the girder and the roller in his modeling based on Iowa River bridge erection data (Wipf et al., 2004) and this did not reflect the real contact condition.

The primary objective of this study is to estimate the relationship of the maximum contact stress between an I-girder and a roller using a nomogram. The proposed nomogram is built based on a parametric study by numerical modeling with various roller dimensions and loads. The maximum contact

stress from the nomogram can be estimated quickly and with ease and the nomogram could be a useful tool for predicting the maximum stress between a bridge girder and a support system. This study includes preliminary modeling of the cylindrical contact to validate the Hertz contact theory. In addition to that, the field data that was collected during the Iowa River Bridge construction was used to verify the numerical modeling output. Since there are many factors to be considered in modeling, simplified numerical models were developed and compared with the initial numerical modeling. Lastly, a parametric study was performed with various roller diameters, roller width, and vertical load to build a nomogram, which can be used to estimate the maximum contact stress at the contact region.

2. Methodology

2.1 Numerical Modeling of Hertz Contact

As a preliminary study, a numerical model featuring a small-scale cylinder in contact with a plane (see Fig. 1) was developed in ANSYS® to verify the applicability of the Hertz contact stress theory (see Equations (1) and (2)). The data used were: force (F) of 2,500 lb_f (11,120 N), contact length (l) of 3 inches (76.2 mm), cylinder diameter (d_1) of 18 inches (457.2 mm), the diameter of the plane surface (d_2) was defined as infinite, Elastic Modulus (E) of 29,000 ksi (200 GPa) for the steel cylinder and the plane, Poisson's ratio (v) of 0.3 for both objects, and the depth of contact surface (z). In order to optimize result accuracy, mesh refinement was continually utilized. Consequently, the validity of the model was improved until the contact stress obtained differed from the Hertz contact theory by less than one percent. The common mesh type in ANSYS® modeling consists of tetrahedral and hexahedral shapes. The tetrahedral mesh does not have constraints in terms of component styles and a specified pattern generated to the numerical modeling, but unstructured tetrahedral meshing also requires more elements than a hexahedral dominant mesh. Typically, hexahedral meshes have advantages over tetrahedral finite element meshes such as reduced error, smaller element numbers, and increased reliability. However, the hexahedral finite element mesh generation has a limitation in terms of the geometry shape. The hexahedral mesh includes the pattern of the meshing and technically takes more effort to generate the style (Chang, 2004b). In this study, the hexahedral mesh generation for numerical modeling was applied in modeling as shown in Fig. 1 (a).

Hertz contact theory assumes that structures behave are within their respective elastic limits and there is no friction on the contact surface. The contact line is a linear feature when two separate surfaces touch each other. In numerical modeling, one side of a contact pair is deemed as the contact part while the other surface is defined as the target part. Typically, solid contact surfaces do not interpenetrate with each other. Therefore, ANSYS® generates a relationship between the two surfaces in the models to control them from penetrating each other during the simulation process. It can identify reasonable contact pairs by presenting contact parts. Moreover, ANSYS® provides different contact pair elements, such as node-to-node, node-to-surface, and surface-to-surface. The contact area is loaded at the target surface where penetration is expected. Contact surfaces provide a wide range of types of interactions between elements in geometry. In this research, surface-to-surface contact was used to identify the contact pair elements. The contact area of the cylinder is defined as a contact surface while the plane surface represents a target surface.

The results obtained from the Hertz contact theory (Hertz, 1896) between the cylinder and the plane surfaces include contact patch width (Equation 1) and maximum contact stress (Eq. (2)).

$$b = \sqrt{\frac{2F((1-v_1^2)/E_1 + (1-v_2^2)/E_2))}{\pi l\left(\frac{1}{d_1}+\frac{1}{d_2}\right)}} \tag{1}$$

$$p_{max} = \frac{2F}{\pi bl} \tag{2}$$

where b=The Half Contact Patch Width, F=Force, v= Poisson's Ratio, E= Elastic Modulus, d=Diameter, p_{max}= The Maximum Hertz Contact Stress, l=Contact Length.

The contact stress of the numerical model was then compared to the theoretical results from Hertz contact theory. In the numerical model (see Fig. 1 (b)), the maximum contact stress between the plane and the cylinder was 21.55 ksi (148.6 MPa), which is in line with the maximum stress of 21.67 ksi (149.4 MPa) obtained by way of Hertz contact theory. The difference between two values is approximately 0.6%.

3. Numerical Modeling of Iowa River Bridge

The incremental launching method (ILM) is one of the erection methods used for bridge construction in environmentally sensitive areas. This method is performed by constructing parts of the steel girders behind an abutment, linking them together, and pulling or pushing the assembled segments on support bearings to their permanent location. During the launch, contact stress can be generated between a roller and a girder as mentioned earlier.

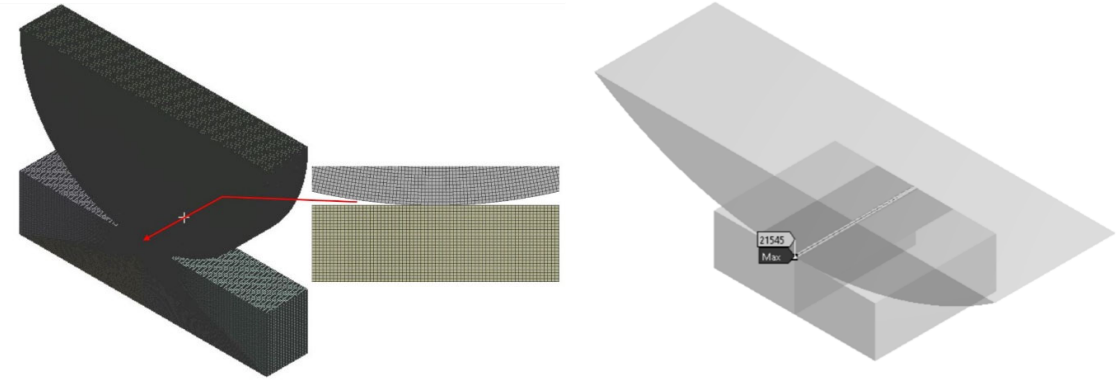

(a) Hexahedral mesh (b) Contact stress between two surfaces (psi)

Fig. 1. Numerical modeling of contact stress for a cylinder in contact with a plane

The Iowa River Bridge (IRB) consists of four steel plate I-girders (shown in Fig. 2), each of which is approximately 11 ft (3.4 m) deep and each of the five spans has a length of 302 ft (91.7 m) over six piers. In order to support the steel girders within the launch pit, four temporary rollers, notated as RA, RB, RC, and RD, were installed behind Pier 6. Fig. 2 (a) describes the locations of piers 1 to 6 and plans the view of the launching girders. The steel girders were arranged to start in a launching area located east of Pier 6 while the temporary steel tapered launch nose was attached to the two interior girders and had a length of 146.5 ft (44.7 m). These nose parts were connected to two steel girders that were in vertical and longitudinal alignment with the two interior girders for the IRB. The nose assembly was used to control the launching girders upward over each pier. The steel frame launching tail assembly is 24 ft (7.3 m) long and temporarily connected to the end of launching girder (Fig. 2 (a) and (b)). The detailed elevation views of the girder at launching distance 823.5 ft. Contact-strain data were collected during the launching of the westbound roadway of the IRB Girder C. The instrumentation was installed on the cross-section at the point of highest contact stress (where it passed over Pier 6 (Fig. 2 (c))).

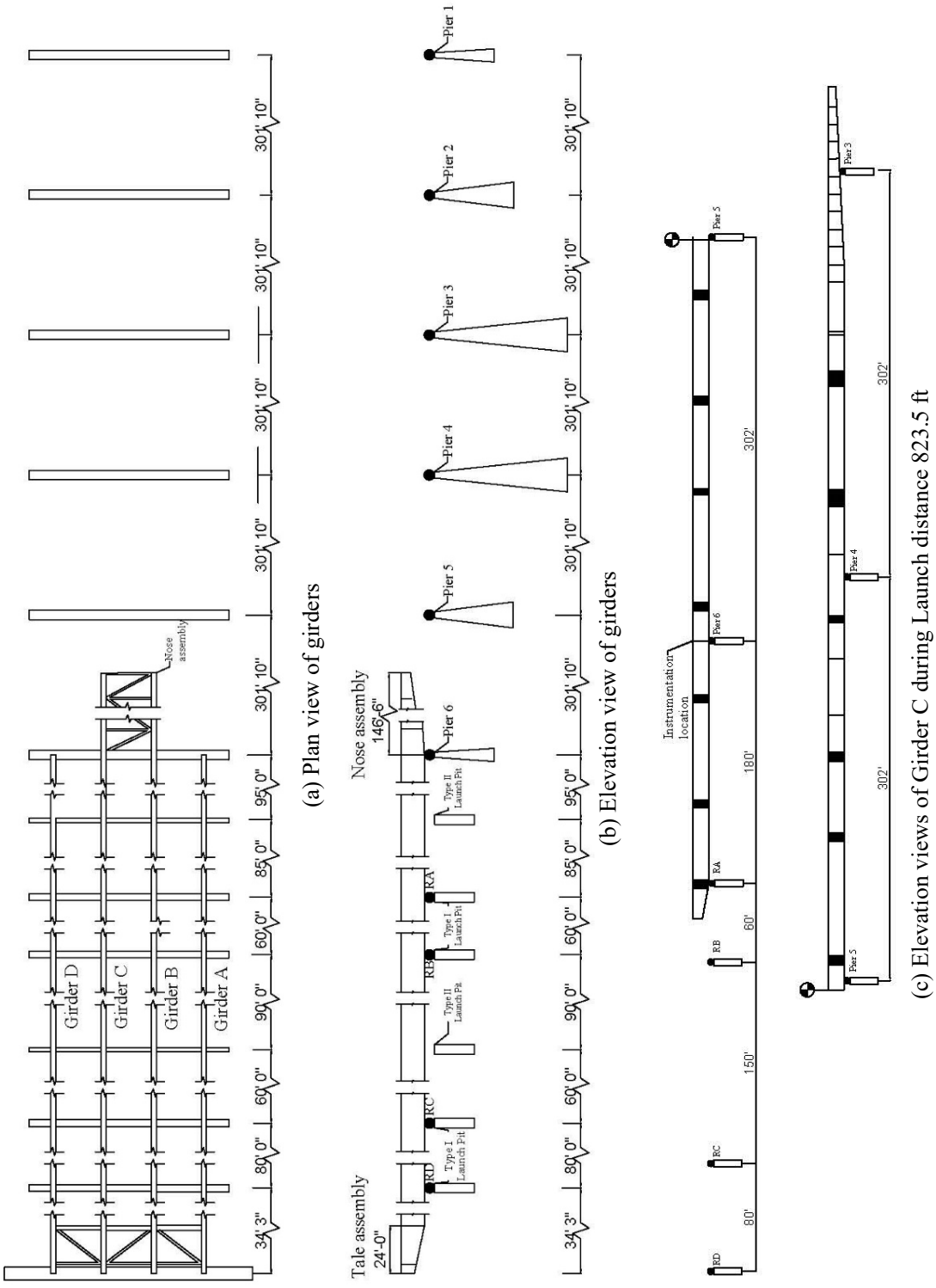

Fig. 2. General launching description of Iowa River Bridge

A numerical modeling was developed in an equivalent way that was used for Hertz contact modeling discussed in the previous section and the field strain measurement during the launch of the IRB Girder C at a stage of 823.5 ft and numerical modeling were compared. The cross section of the IRB Girder C has a web of 135-⅞ inches (3451.2 mm) by ⅞ inches (22.2 mm), top flange of 14-¾ inches (374.7 mm) by ⅞ inches (22.2 mm), and a bottom flange of 19-⅝ inches (498.4 mm) by 1-¼ inches (31.8 mm) (Fig. 3 (a)). A total of 13 strain gages were installed on the lower parts of the Girders C (Wipf T, 2004). The strain gage names represent a specific point on the girder. For example, CS represents Girder C and

Southern side, CN represents Girder C and Northern side, BW represents Bottom gages on the Web, IF represents Inner gages on the Flange and OF represents Outer gages on the Flange, OBF represents Outer gages on the Bottom Flange (Fig. 3 (b)). The lower surface of the girder bottom flange was in contact with the roller support surface. The roller has a diameter of 18 in. (457.2 mm) and a width of 6 in. (15.24 mm).

The numerical model was developed for the relevant portion of the girder. The model includes geometry and material properties, mesh generation, girder-aspect ratio, and member end forces, which were set to validate the field measurement. Additionally, the following assumptions were made: the girder cross-section is constant; only static load emanates from the self-weight; and the steel roller is supported at the center of the steel girder during launching.

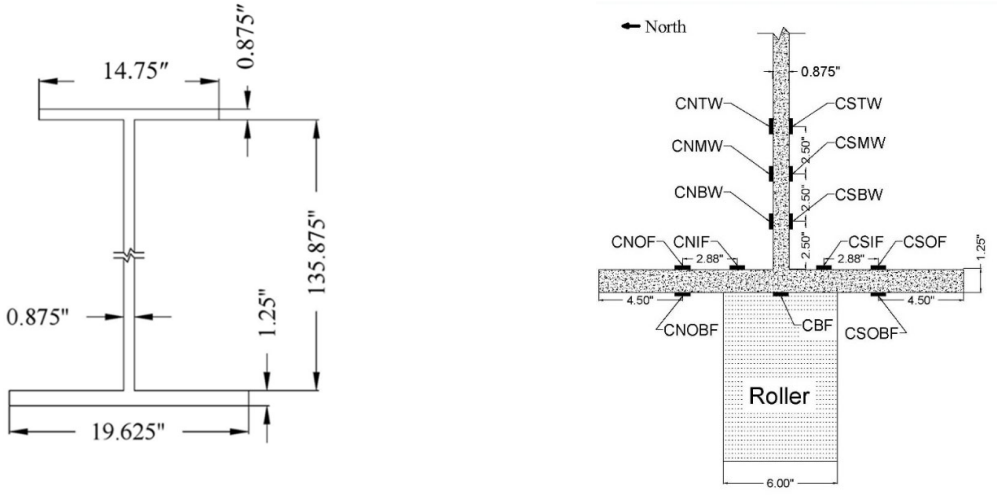

(a) Girder C cross-section (b) Strain gage positions

Fig. 3. Girder C cross section and strain gage locations
Note: 1 inch = 25.4 mm

3.1 Geometry and material properties

Since the IRB Girder C is symmetric in terms of geometry, load, and constraints, the numerical model reduces the size of geometry and complexity of the model. Therefore, one half of Girder C and the roller were modeled in ANSYS®. The contact-pair concept was applied between the surface of the roller and the lower surface of the bottom flange. The material properties for the selected element are similar to steel: density of 490 lb/ft^3 (7849 kg/m^3) a modulus of elasticity of 29,000 ksi (200 GPa), a yield strength of 50 ksi (345 MPa) and 36 ksi (250 MPa) for the girder and the roller, respectively, and a Poisson's ratio of 0.3 (Chang, 2004b).

3.2 Mesh generation

The hexahedral mesh can be generated for the complex geometries by finite element analysis. In addition to that, mesh density between contact areas is found to influence the reliability of the numerical model's results. To standardize the contact area analysis, a mesh style with small element sizes for all the configurations is chosen. The use of hexahedron elements can reduce the time needed to generate the mesh, which is advantageous in reducing the number of elements and reliability improvement (Shepherd, 2006). In the model, the hexahedral mesh was generated with a high density around the contact area (between the lower surface of the bottom flange and roller) which is significant for achieving accurate contact strain results and minimizing computational processing time. For this study, the numerical model

has a total of 2,299,747 nodes and 506,994 elements. The minimum mesh size at the web interface and the flange of the Girder C was approximately 0.1 in. (2.5 mm), which has a direct influence on the reliability of the solutions.

3.3 Girder-aspect ratio

Elementary-beam theory assumes the length of a span is significantly larger than the depth of the section. Since the entire girder is too large to analyze in three-dimensional modeling, only a portion of girder was analyzed. According to Chang's study (2004b), the most effective girder-aspect ratio in the analysis was determined to be 6. The girder-aspect ratio defines the ratio between the length and depth of the girder. The member-end forces at both end sections were obtained using a simple beam (line) analysis in STAAD Pro®. For simplicity, the nose and tail assemblies were assumed to be half the weight of Girder C in the beam analysis. Fig. 4 illustrates the structural behavior and internal forces after a launching the superstructure for 823.5 ft when the instrumented section was directly positioned over the roller at Pier 6.

3.4 Member end forces

Shear forces and bending moments were collected 34.5 ft (10.5 m) away from Pier 6 on both the left and right sides by considering a girder-aspect ratio of 6. The half value of the shear forces V_L of -46.64 kips (-207.5 kN), V_R of 59.56 kips (264.9 kN) and bending moments M_L of -1375.87 kip·ft (-1865.4 kN·m), M_R of -930.02 kip·ft (-1260.9 kN·m) were applied as the member-end forces to both sides due to symmetric geometries. Also, the self-weight (W) of the steel girder and roller were both considered in the modeling. The boundary condition for this analysis is a fixed support that was applied at the bottom surface of the half roller (R) (see Fig. 5). The friction contact between surfaces was applied to the numerical model with a friction coefficient of 0.3. For the IRB Girder C contact analysis, half of the lower surface of the bottom flange was defined as a target surface while half of the roller surface was defined as a contact surface. The total solution time required for numerical modeling was approximately 6 hours using an Intel® Core™ i7-7700 processor (CPU@ 3.6 GHz and RAM capacity of 32 GB).

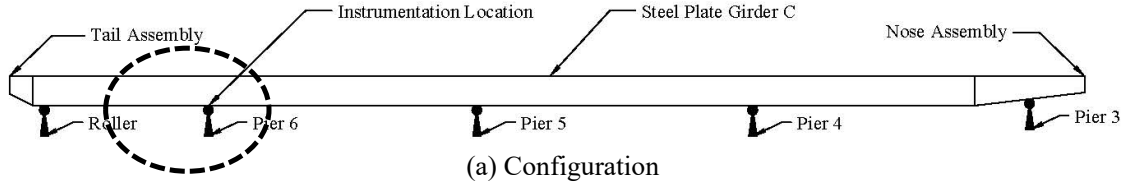

(a) Configuration

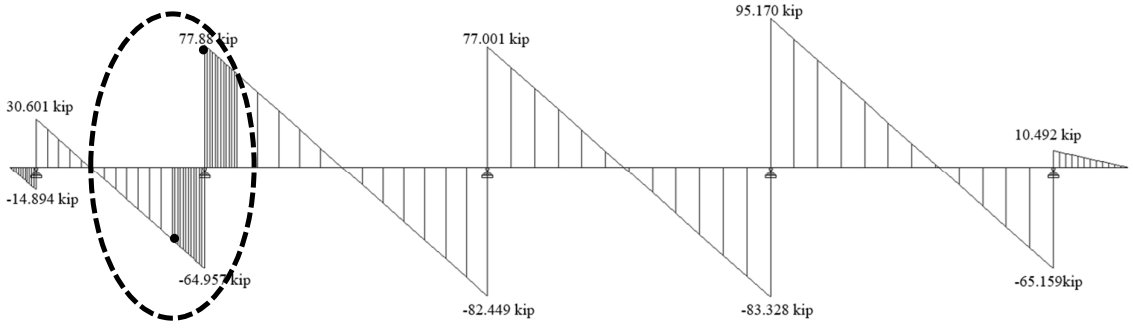

(b) Shear diagram (F_y)

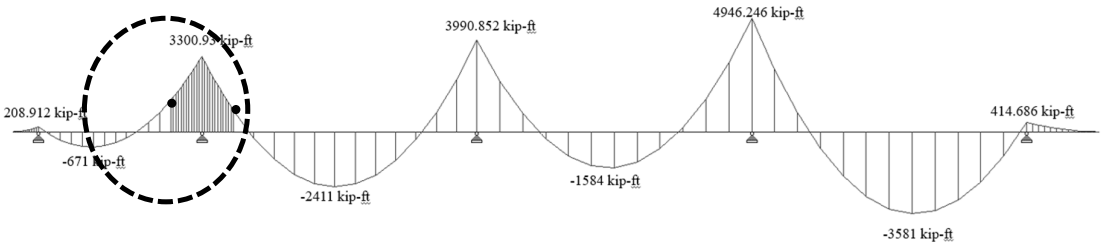

(c) Bending moment diagram (M_z)

Fig. 4. Beam analysis of Girder C at stage 823.5 ft
Note: 1 kip = 4.45 kN and 1 kip-ft = 1.36 kN-m

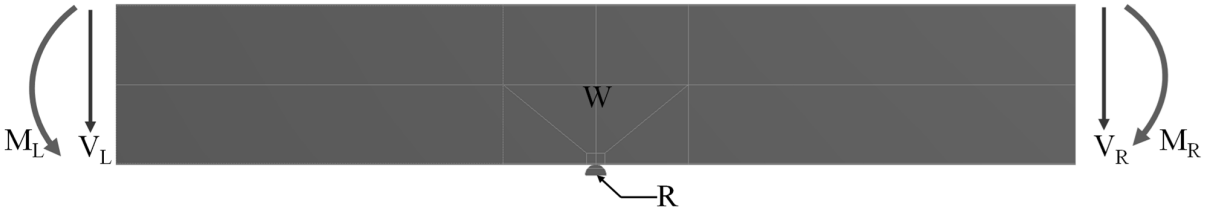

Fig. 5. Girder segment used for the contact stress analysis

Since there are several strain gauges installed, selected strains (CBW and CBF) were compared. Fig. 6 (a) shows the predicted vertical strain (CBW) in the web of Girders C located near Pier 6 from the numerical modeling and the field data. As shown in the figures, the numerical modeling results illustrate a similar pattern to the field measurements. The strain at the center strain gauge of the bottom flange (CBF) at a launch distance of 823.5 ft increases up to 4390 micro-strains (μ) in compression according to the field data while in the numerical model, the value is 2870 μ (see Fig. 6 (b)). The strain values measured from CBF could be a combination of the flange strain and gauge strain due to the excessive pressure by the roller. The extreme strain data from the CBF could be measured beyond stage 823.5 ft due to the gauges being destroyed when they encountered the roller. This comparison reveals the significance of numerical modeling for contract stress.

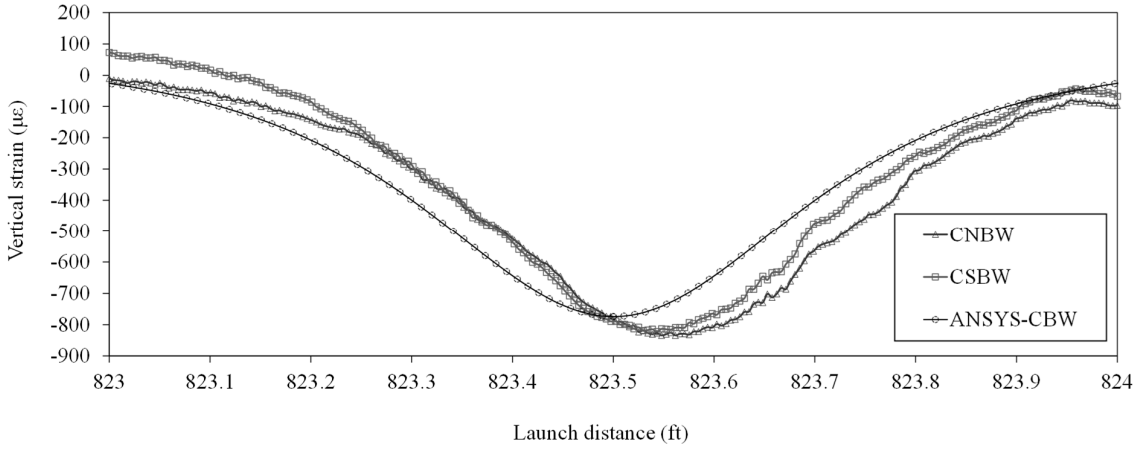

(a) Bottom gages on the Web

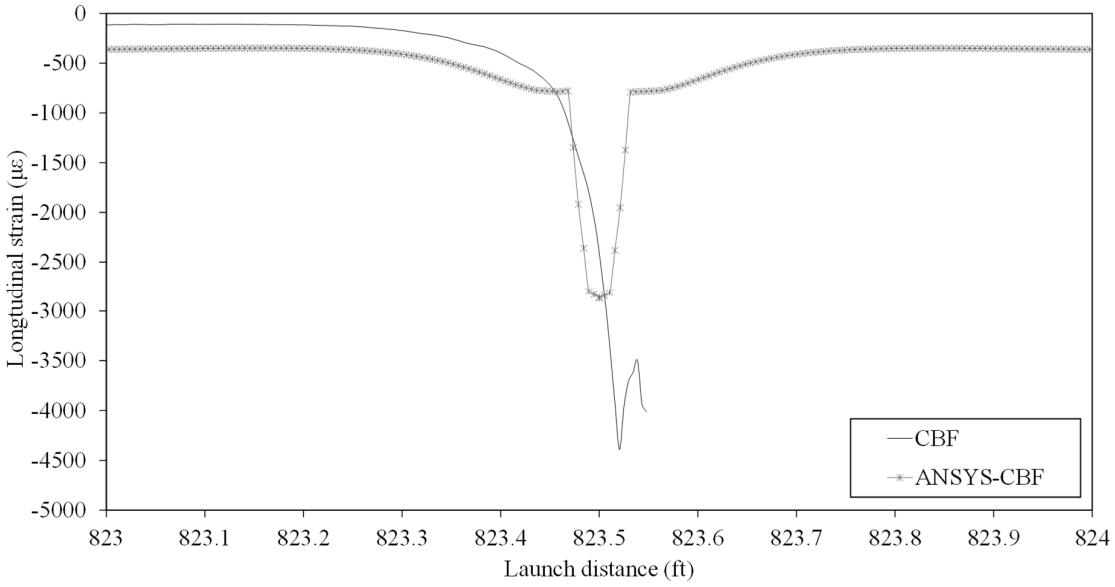

(b) Longitudinal strain at the center strain gage of the bottom flange (CBF)

Fig. 6. Comparison between the field data and numerical modeling from 823 to 824 ft

4. Results

4.1 Simplfied Contact Modeling

Since the internal forces vary depending on the girder stage, it is not easy to modify the input data in the numerical model for each analysis. In addition, according to the Hertz contact theory, the most significant factor of contract stress is the vertical force. Thus, the numerical model for the IRB contact stress was simplified and the results were compared with the previous numerical model and the field data again. The following assumptions toward the simplified numerical modeling were considered: the girder is assumed to have an aspect ratio of 6; the model is symmetric in loading, geometry, and boundary conditions; the roller is positioned at the center of the girder bottom flange; and only the roller reaction impacts the contact stress significantly while bending moment is ignored. Similarly, half of the roller surface is modeled as a contact surface and half of the lower surface of the bottom flange is defined as a target surface. The contact friction of 0.3 is applied between the contact surfaces. However, the reaction from the previous model including both end shear forces, and self-weight were applied at the bottom of roller in the simplified contact modeling. The boundary condition in the modeling includes a fixed top surface of the flange (see Fig. 7).

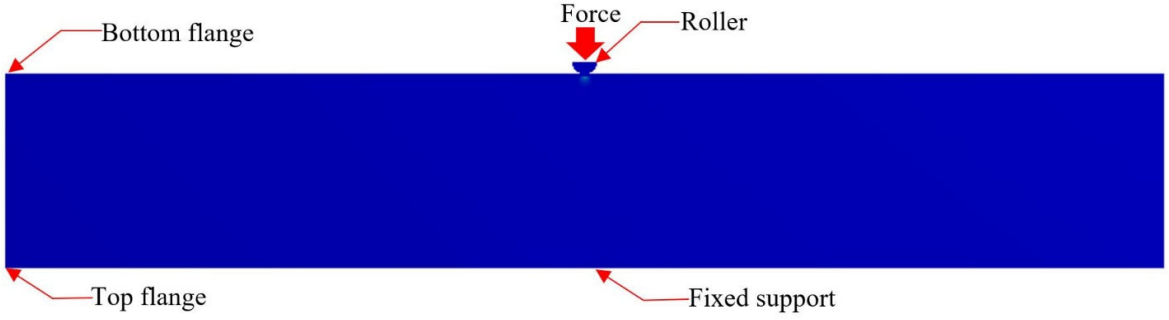

Fig. 7. Geometry of simplified numerical modeling

The IRB Girder C contact modeling (the original modeling) and simplified modeling were developed with a hexahedral mesh and compared with the field data. The longitudinal strains of the lower surface of the bottom flange are compared between the launching stages from 823 ft to 824 ft. Both predicted longitudinal strains for the original modeling and simplified modeling at the center strain gauge (CBF)

on the lower surface of the bottom flange follow a similar trend of the field data as shown in Fig. 8. The maximum predicted longitudinal strains at CBF from simplified modeling is approximately 2725 μ while the previous numerical model showed approximately 2870 μ. This shows about 5% difference and indicates that the primary factor of contact stress is the vertical force while the bending moment is minimal in contact stress between a bridge girder and a support roller.

4.2 Contact Stress Nomogram

Since numerical modeling is not always applicable and convenient, this study focuses on an approximate solution to estimate the contact stress between a bridge I-girder and a support roller. A nomogram is a proposed method to provide approximate contact stress. To develop a nomogram, about 140 simplified numerical models were generated with different variables as a parametric study. The variables considered in creating the nomogram are vertical reaction, the roller diameter and roller with (contact length) based on the hertz contact theory. Table 1 shows part of data that was used in the development of the proposed contact stress nomogram. The range of load is from 5 kips (22.2 kN) to 25 kips (111.2 kN), the roller diameter increases from 14 inches (355.6 mm) to 22 inches (558.8 mm), and the roller width considered is from 5 inches (127 mm) to 8 inches (203.2 mm).

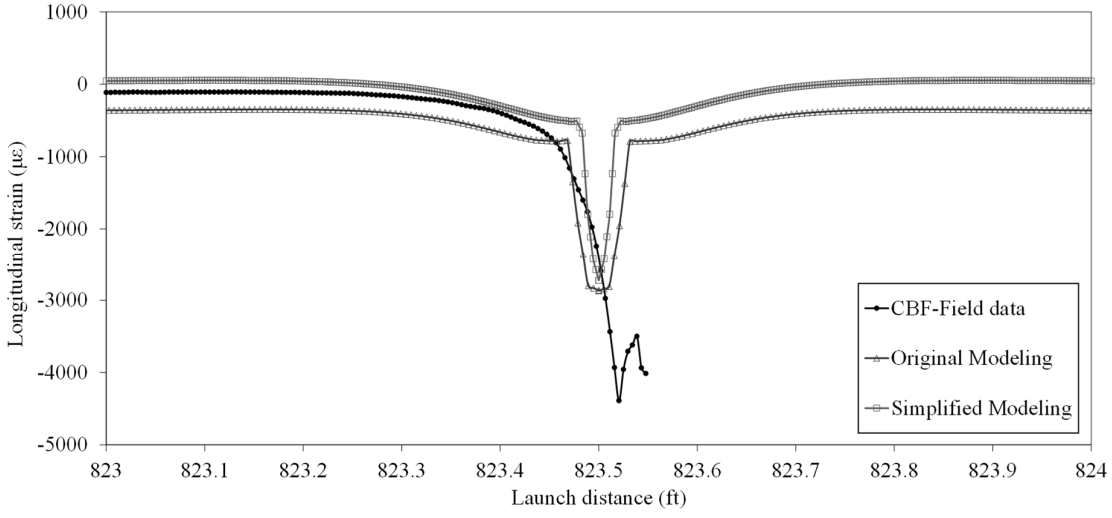

Fig. 8. Longitudinal strain in the lower surface of the bottom flange from 823 ft to 824 ft

The proposed nomogram consists of four parallel scales as shown in Fig. 9. The leftmost and right-side scales are designated the input variables, consisting of the roller profile and total load identifying their values. The middle scale on the left side of the turning axis (T) represents the designated maximum contact stress for the input variables in simplified modeling. The advantage of the proposed nomogram is ease of solution determination and quick estimation of maximum contact stress in the bridge girder. However, the numerical model used for the nomogram was based on linear analysis and if the maximum contact stress is above the yield strength of the material, the nomogram is not applicable to define the contact stress. Further numerical modeling is required for the case. To determine the approximate maximum contact stress using the proposed nomogram, the following steps are required. First, locate measuring length of contact (roller width) and force on the appropriate scales and connect these points until the turning axis (T) is intersected. Next, locate the roller diameter and connect with the intersected T axis. Finally, read the maximum contact stress to be expected with thin contact area. For example, for a force of 15 kips, a contact length (roller width) of 6 inches (125.4 mm), and a roller diameter of 18 inches (457.2 mm), the maximum contact stress meets a value of 50 ksi (344.74 MPa) (see blue dash line in Fig. 9). As another example, a force of 5 kip (22.24 kN), a contact length (roller width) of 5 inches (127 mm), and a roller diameter of 22 inches (558.8 mm) are provided, then the maximum contact stress between roller and bottom surface of the steel I-girder is determined to be approximately 18 ksi (124

MPa) (see solid black line in Fig. 9). If a force of 25 kip (111.21 kN), a contact length (roller width) of 8 inches (203.2 mm), and a roller diameter of 14 inches (355.6 mm) are provided, then the maximum contact stress is approximately 70 ksi (482.63 MPa) (see solid red line in Fig. 9).

Table 1. Parametric study

(a) A constant roller width of 6 inches (152.4 mm)

Variables			Numerical Modeling
Roller width (in.)	**Force (kip)**	**Roller diameter (in.)**	**Maximum contact stress (ksi)**
6	5	14	18.06
6	5	16	17.58
6	5	18	16.57
6	5	20	16.08
6	5	22	15.80
6	10	14	36.11
6	10	16	35.17
6	10	18	33.14
6	10	20	32.16
6	10	22	31.60
6	15	14	54.17
6	15	16	52.75
6	15	18	49.71
6	15	20	48.23
6	15	22	47.40
6	20	14	72.23
6	20	16	70.34
6	20	18	66.28
6	20	20	64.31
6	20	22	63.19
6	25	14	90.28
6	25	16	87.93
6	25	18	82.86
6	25	20	80.38
6	25	22	78.99

Note: 1 inch = 25.4 mm, 1 kip = 4.45 kN, and 1 ksi = 6.9 MPa

(b) A constant roller diameter of 18 inches (457.2 mm)

Variables			Numerical Modeling
Roller width (in.)	**Force (kip)**	**Roller diameter (in.)**	**Maximum contact stress (ksi)**
5	5	18	21.50
6	5	18	16.57
7	5	18	15.67
8	5	18	11.23
5	10	18	43.00
6	10	18	33.14
7	10	18	31.33
8	10	18	22.45
5	15	18	64.50
6	15	18	49.71
7	15	18	43.22
8	15	18	33.68
5	20	18	86.01
6	20	18	66.28
7	20	18	57.62
8	20	18	44.90
5	25	18	107.51
6	25	18	82.86
7	25	18	70.08
8	25	18	56.12

Note: 1 inch = 25.4 mm, 1 kip = 4.45 kN, and 1 ksi = 6.9 MPa

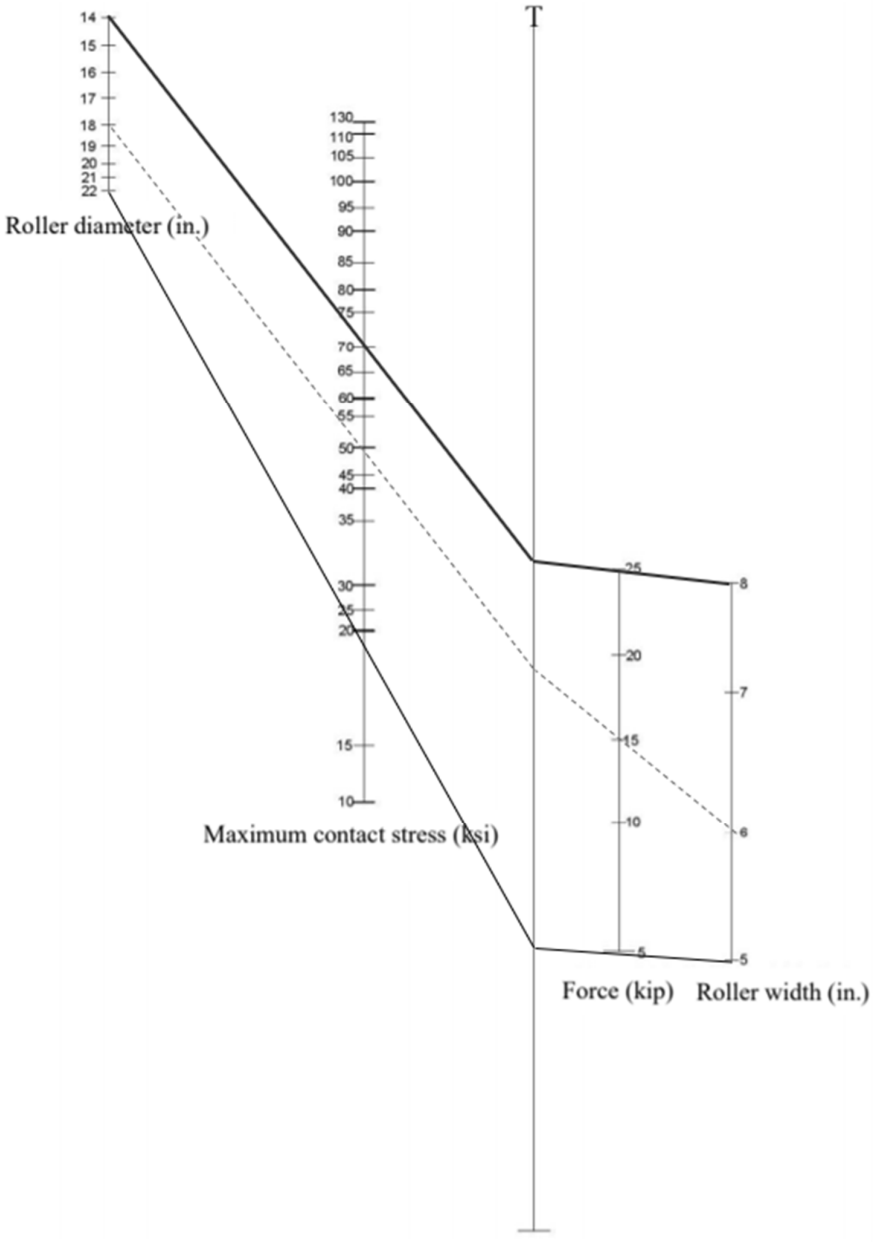

Fig. 9 Maximum contact Stress nomogram (E=29,000 ksi, ν=0.3)
Note: 1 inch = 25.4 mm, 1 kip = 4.45 kN, and 1 ksi = 6.9 MPa

5. Conclusion

The primary objective of this study is to estimate the relationship of the maximum contact stress between an I-girder and a roller using a nomogram. The proposed nomogram is built based on a parametric study with various roller dimensions and loads by numerical modeling. This study began with preliminary modeling of the cylindrical contact to validate the Hertz contact theory and followed by validation modeling with Iowa River Bridge. A parametric study with simplified numerical modeling was performed with various roller dimensions and load to build a nomogram. Most of the following conclusions have been verified using numerical modeling. Mesh style and size near the contact region are significant to improve the numerical modeling results. The crucial factors for contact stress between a steel girder and a roller are: force near the contact area; roller diameter; and contact width. The vertical force impacts the contact stress significantly while the bending moment is minimal. The proposed nomogram is quick and easy to use and is applicable to estimate the approximate contact stress between a gider and a support roller in the elastic stage.

References

Bekheet, N. (2017). Involute Gear Tooth Stresses Analysis Using Finite Element Modeling. *Journal for Engineering, Technology, and Sciences*, *34*(1). 269-284.

Chacón, R. U. (2013). Numerical Validation of the Incremental Launching Method of a Steel Bridge Through a Small Scale Experimental Study. *Experimental Techniques, 40*, 333-346. https://doi.org/10.1007/s40799-016-0037-5

Chang, B. (2004a). Analysis of Non-linear Contact Stresses for Launched Plate Girder Bridges. *Transportation Scholars Conference, Ames, Iowa*.

Chang, B. (2004b). Recommendations for the Analysis of Contact Stresses for Launched Plate Grider. *Mater's Thesis, Iowa State University, Ames, Iowa*.

Donzella, G. & Petrogalli, C. (2010). A failure assesment diagram for components sujected to rolling contact loading. *International Journal of Fatigue*, *32*, 256-268. https://doi.org/10.1016/J.IJFATIGUE.2009.06.016

Gąska, D., Haniszewski, T. & Margielewicz, J. (2017). I-beam girders dimensioning with numerical modelling of local stresses in wheel-supporting flanges. *Mechanika, 23*(3), 347–352. https://doi.org/10.5755/j01.mech.23.3.14083

Granath, P. (1997). Behavior of Slender Plate Girders Subjected to Patch Loading. *Journal of Constructional Steel Research*, *42*(1), 1-19. https://doi.org/10.1016/S0143-974X(97)00021-7

Granath, P. (1998). Distribution of Support Reaction Against a Steel Girder on a Launching Shoe. *Journal of Constructional Steel Research*, *47*(3), 245-270. https://doi.org/10.1016/S0143-974X(98)00006-6

Gupta, B, Abhishek, C., & Gautam, V. (2012). Contact Stress Analysis of Spur Gear. *Journal of Engineering Research & Technology*, *1*(4), 1-7.

Hertz, H. (1896). The Principles of ,Mechanics, Miscellaneous Papers. *Macmillan & Co., London, U.K*.

Laukkanen, A., Holmberga, K., Ronkainen, H., Stachowiak, G., Podsiadlo, P., Wolskib, M., Gee, M., Gachot, C. & Li, L (2017). Topographical orientation effects on surface stresses influencing on wear in sliding DLC contacts, Part 2: Modelling and simulations. *WEAR*, *389*(15), 18-28. https://doi.org/10.1016/j.wear.2017.03.026

Norden, B. (1973). On the Compression of a Cylinder Contact with a Plane Surface. *Institute for Basic Standards National Bureau of Standards. Washington , D.C.*

Olver, A. V. (2005). The machanism of rolling contact fatigue: an update. *Proceedings of the Institution of Mechanical Engineers, Part J: Journal of Engineering Tribology, 219(5)*, 313-330. https://doi.org/10.1243/135065005X9808

Rogač, M., Aleksić, S. and Alesksic, D. (2020). Influence of patch load length on resistance of I-girders. Part-I: Experimental research. *Journal of Constructional Steel Research*, 175. https://doi.org/10.1016/j.jcsr.2020.106369

Rogač, M., Aleksić, S. and Alesksic, D. (2021). Influence of patch load length on resistance of I-girders. Part-II: Numerical research. *Journal of Constructional Steel Research*. https://doi.org/10.1016/j.jcsr.2020.106388

Shepherd, J. F. & Johnson, C. R. (2008). Hexahedral Mesh Generation Constraints. *Engineering with Computers* , 24, 195–213. https://doi.org/10.1007/s00366-008-0091-4

Wen, Z., Wu., L., Li, W., Jin, X. & Zhu, M. (2010). Three-dimensional elastic–plastic stress analysis of wheel–rail rolling contact. *Wear, 271*(1)*, 426-436*. https://doi.org/10.1016/j.wear.2010.10.001

Wipf, T., Phares, B., Abendroth, R., Wood, D., Chang, B. & Sbraham, S. (2004). Monitoring of the Launched Girder Bridge over the Iowa River on US 20. CTRE Project 01-108, Iowa State University, Ames, IA.

Wriggers, P. (1996). Finite Element Methods for Contact Problems with Friction. *Tribology International*, *29*(8), 651-658. https://doi.org/10.1016/0301-679X(96)00011-4

Zhao, X. & Li, Z. (2015). A Three-dimensional Finite Element Solution of Frictional Wheel–rail Rolling Contact in Elasto-plasticity. *Journal of Engineering Tribology*, *229*(1), 86–100. https://doi.org/10.1177/1350650114543717